A Self-Commutated Helical Polypyrrole Actuator Fabricated by Filament Patterning

Kadri-Ann Valdur, Tarmo Tamm, Alvo Aabloo, and Indrek Must

***Abstract*—Reversible retaining attachment is a universal task in which bioinspired soft robotic solutions in the form of a helix may come in handy. In this letter, we propose an mm-scale non-metallic electroactive polymer (polypyrrole) helical actuator with a 3D multimode (elongation, rotation) actuation with elastomer-like anchorage retainment. The non-reconfigurable bonds formed by electrodepositing polypyrrole on a temporary 3-D coiled-filament template programmed its shape. Filament-induced fracturing during template removal finalized the helix shape. Anisotropy introduced in the synthesis process yielded a helix with 8% linear strain, up to ≈180° tip rotation, and 63% structural strain. The self-commutated spirals of the helix played a critical role in the super-structure of the actuator with charge transfer and commutation-induced bi-stable motion. The potential applications include reversible compliant anchoring solutions for biomaterial (e.g., bacteria) scaffolding in bio-hybrid robots.**

***Index Terms*—Automation at micro-nano scales, compliant joints and mechanisms, grasping, soft robot materials and design.**

I. Introduction

REVERSIBLE attachment and compliant grip retainment (such as in Velcro) are the gateway from traditional stationary (bio)scaffolding to biohybrid robotics. Living guest systems (e.g., cells, bacteria) can benefit from much more than simple mechanical fixation: the scaffold holding a biomaterial can stimulate function or growth, e.g., via mechanical [1] and electrical [2] stimulation. In addition, the scaffold needs to adapt to changing configurations for various applications (e.g., reconfigurable surgical grippers that respond to specific chemicals [3]), rendering the geometrical arrangement of paramount importance.

In a helical construct, a single motor unit drives the device to a variety of motions such as bending, twisting, coiling, and length change [3], which could be beneficial for reversible attachment due to the simultaneously engaged modes. In nature, the relatively simple shape of a helix appears in surprisingly many places – from molecular scale (DNA) to plant attachment organs (tendrils), seashells, and horns [4], and possibly in human muscle operation [3]. The community has seen this potential for bioinspired robotic applications [3], and work is ongoing with artificial muscles based on simple materials such as fishing line and sewing thread powered by helixes [5], helical yarn actuators [6], variable stiffness helical grippers [7] and microswimmers [8], [9].

Creating a helical actuator is relatively easy– e.g., twisting and fixing a functional ribbon around a tubular support. However, attractive low-voltage-driven (easy to control) electroactive polymers (namely conductive polymers – CPs) that enable small-scale actuators are non-thermoplastic. This gives CPs such as polypyrrole (PPy) high stability in shape, but also excludes post-synthesis shaping processes such as extrusion. Electrochemical synthesis of PPy allows for encoding response characteristics (e.g., optimized for anion or cation mobility) by varying input parameters (current density and potential) and electrochemical cell components (electrode material, electrolyte, solvent, synthesis time, additives) [10], [11].

Polypyrrole (PPy) is a CP with renowned use in small-scale robotics due to its relatively significant volume change in response to electric stimuli during oxidation/reduction [12], high conductivity [10], and biocompatibility enabling biomedical applications [13]. Examples of exceptional bioscaffolding potential include PPy used as a coating for colonizing bacteria in microbial fuel cells [14]; monitoring bacterial activity [15], and even differentiating types of guest bacteria at a PPy host [16]; electrical [2] and mechanical [1] cell stimulation. Prior 3D helical structures of PPy include spirulina templated helixes [17], magnetic microswimmers [18], and flattening spirals [19]; building on this, we show a PPy-helix formed electrochemically on a central beam via filament patterning.

We consider the potential scenario of the PPy helical scaffold as follows. First, the gripper achieves a binary (i.e., successful or not) anchorage by coupled electromechanical rotation and elongation (Fig. 1, Phase I), the tip of the helix tracks a helical path. Possible anchored objects include unstructured environments such as (hooked) textile, mesh, and knobs. Consequently, the helix can comply with the movements and growth of the guest organism by reversible elongation (Fig. 1, Phase II); the compliance is here determined by structural elasticity of the helix, promising structural strains much beyond that of a column. Finally, the helix can release its guest system by shortening and unwinding as a result of applied current density opposite to that of Phase I (Fig. 1, Phase III), highlighting the recovery and repeatability of our system.

Manuscript received October 11, 2021; accepted March 3, 2022. Date of publication March 23, 2022; date of current version April 6, 2022. This letter was recommended for publication by Associate Editor C. Cao and Editor K. Cho upon evaluation of the reviewers' comments. This work was supported in part by Estonian Research Council under Grants PRG1084 and PRG1498 and in part by H2020 project TWINNIMS under Grant Agreement Number 857263. *(Corresponding author: Kadri-Ann Valdur.)*

The authors are with the Institute of Technology, Intelligent Materials and Systems Lab, University of Tartu, 50411 Tartu, Estonia (e-mail: kadri-ann.valdur@ut.ee; tarmo.tamm@ut.ee; alvo.aabloo@ut.ee; indrekm@ut.ee).

Digital Object Identifier 10.1109/LRA.2022.3161694

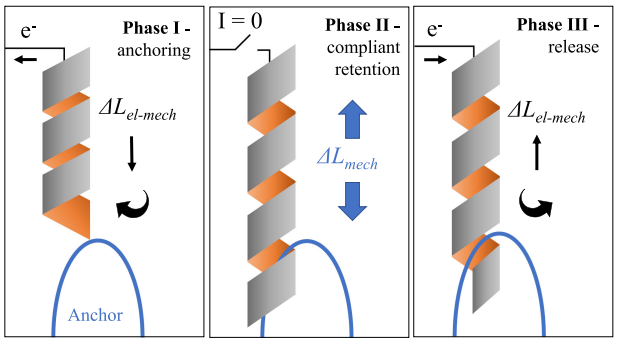

Fig. 1. The concept of the anchorage of the PPy-helix. In Phase I, the anchoring is achieved with electromechanical strain induced by charge, resulting in strain and tip rotation via the increase in the amount of turn. During Phase II, the anchorage is retained due to the high compliance of the PPy-helix, allowing for mechanical straining. Phase III concludes the operation cycle with reversible release.

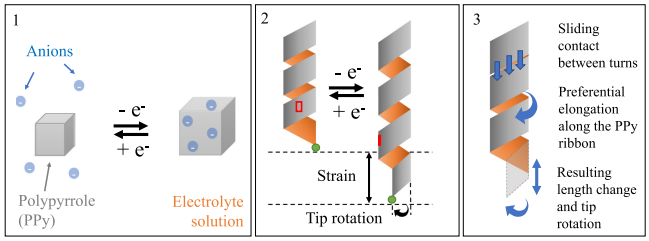

Fig. 2. Level 1: Material. Anion-active system actuation. A piece of PPy is connected to a power source that drives the actuation of the PPy with an electric charge (current). With a positive current, the anions are pulled inside the PPy, causing a positive volumetric effect. The effect is reversible: negative current expels the anions from the PPy matrix, causing shrinkage. Level 2: Geometry. Working principle of the helical multimode actuator. The red rectangle and the green dot drawn on the surface and at the helix tip help visualize the actuator's elongation and coiling with the positive volumetric change induced by the positive current. Level 3: Super-structure. The self-commutation between the helix's spirals amplifies the structure's overall strain.

The novelty of the work is summarized as follows:

1) Filament induced crack propagation is an effective method to create electroactive structures incorporating sliding surfaces (exampled by a self-commutated helix) of non-thermoplastic electroactive conductive polymer;
2) Helical arrangement of PPy actuator facilitates elastomer-range structural strain while retaining electroactive properties of a non-elastomer CP;
3) Self-commutation between the electrochemically activated helix's coils results in a characteristic tribological behavior, evidenced by a bi-stable actuation profile;
4) Radial material gradient provided by varying the electrical parameters during electrochemical synthesis results in an interface-free bi-layer structure that drives a part of the volumetric change into an additional degree of freedom (tip rotation via increasing the amount of turn at the tip of the actuator).

The actuator's design considerations and working principles are described in Section II. The fabrication and characterization methods are explained in Section III. The results and discussion on the morphology of the helix as well as self-commutation induced friction and bi-stable behavior can be found in Section IV, finishing with concluding remarks in Section V.

II. Design of the Device

Briefly, the **material** – PPy – is electrochemically synthesized in shape, yielding **functional grading** in the growth order upon current density control. Then, the in-shape synthesized material is fractured into a helical **super-structure** by filament-induced cracking directed by the filament's pattern.

A. Material

During injection of electronic charge from an external source to the intrinsically conductive PPy matrix, the electronic charge is compensated by attracting (and reversibly storing) counter-ions from a reservoir (i.e., the electrolyte solution in which the actuator is immersed). The PPy actuation (see Fig. 2, Section I) is governed by an asymmetric conduction mechanism, determined by the selection of synthesis parameters, determining the actuation direction in respect to the injected electronic charge polarity. Both anion-and cation-active systems are possible. This work engages an anion-active system – the anions diffuse into the polymer when charged positively and are expelled from the polymer matrix when charged negatively. The fabrication of PPy via the electrochemical synthesis creates the opportunity to construct actuators that follow the shape of a conductive substrate and yield exceptional control in thickness by simple charge metering. The actuation is an intrinsic material property and does not need assembly (other than a single electrical contact for both synthesis and actuation).

B. Functional Gradients

Synthesis current density determines not only the PPy growth rate but also the structure. A suitably grafted current density waveform enables to create interface-free structures with functionality gradients (effectively interface-free bilayers). In the first approximation, PPy expands isotropically. Applications often require unidirectional expansion; for this, an assembly of several layered bending actuators [20] coil-reinforced tubes [21], fibers, and tubes [11], [22] have been suggested. A bilayer structure, assembled by bonding layers with different volumetric responses, is fundamental for translating an isotropic volume change into a more complex motion: bending of a cantilever or, in our case, coiling/uncoiling of a helix. The electroactive helix designed in this work combines linear and rotary motion modes in a single actuator (see Fig. 2, Section II).

We demonstrate a scalable bilayer formation strategy for a relatively complex 3D shape, i.e., the helix. PPy layer grows gradually in thickness during irreversible electropolymerization, allowing the use of different synthesis parameters (current density) at consecutive growth phases, leading in turn to functional gradients and interface-less layered materials (a similar method has been used to passivate a PPy layer for a bending actuator [23]). A thickness-direction bilayer structure was introduced to

PPy by switching the current density value between two values, resulting in two microstructures:

1) active layer: optimized for volume change;
2) passive layer: inhibited ion mobility and increased stiffness and density, minimally contributing to the volumetric effect.

Fabrication of such a bilayer in a helical shape requires a conductive substrate electrode with a removable 3D template. Patterning is achieved by wrapping a conductive filament around a central beam (electrode). During electrochemical synthesis, the polymer is given a thickness-directional functional gradient (free of delamination issues), translating into a radial gradient when turned into a helix. Filament-induced fracturing caused by the removal of the template results in a PPy ribbon with a close-to-rectangular cross-section shaped like a helix. Post-synthesis fracturing assures self-commutation (sliding surfaces) without sacrificial depositions (as in e.g., lithography) or ablation (by e.g., laser); blade-cutting (as the closest alternative) is estimated to show higher risk of uncontrollable damage due to local stress distribution. With the injection of positive charge, the positive volumetric effect on the outer surface is more significant than in the less-active (passive) inner surface; the resulting stress distribution increases the beam curvature. Charging elongates the PPy ribbon and concurrently increases the amount of turn at the tip.

C. Super-Structure

The chosen fracturing method results in a tightly 'wound' spiral, with adjacent turns close to or in mechanical contact. After synthesis, the PPy structure is transferred from the synthesis solution (containing pyrrole monomers) into an actuation solution (without pyrrole monomers) that induces swelling [11], bridging any cross-turn gaps (see Fig. 2, Section III) and potentially even applying a slight cross-turn tension.

This self-commutation between the turns of the helix is essential for mechanical as well as electrical characteristics with benefits as follows:

1) Linear elongation of the spiral (Fig. 2, Section III) is more pronounced, as the change in volume is not wasted in closing any open gaps along the spiral;
2) The contact electrically commutates the adjacent turns: cross-turn 'shortcut' paths facilitate a faster electronic charge transfer to distal parts of the helix;
3) The sliding surfaces may experience friction, facilitating bi-stable actuation characteristics.

III. Experimental

A. Fabrication

Materials: The chemicals used in this study were as follows. Pyrrole (Py, Aldrich 101527050) was distilled at reduced pressure and kept at -18°C. Tetrabutylammonium hexafluorophosphate (NBu_4PF_6, Fluka 86879), propylene carbonate 99% (PC, Alfa Aesar A15552), and 99.9% lithium bis(trifluoromethane sulfonyl)imide (LiTFSI, Solvionic S001A250) were used as supplied. Platinum (99.9%) wire with a diameter of 0.3 mm was obtained from Alfa Aesar (43014). Tungsten wire with a thin gold layer (Au-W, diameter 33 μm) was used as a spacer on the Pt and as a current collector during synthesis for the optimal cross-section of the resulting PPy-helix ribbon. Stainless steel mesh was used as a counter electrode for electrochemical cleaning and synthesis. For actuation, the counter electrode was a graphite rod. The reference electrodes used were Ag/AgCl 3 M KCl (SmartSens).

Template: The Au-W spacer wire was wound on the Pt wire with an in-house winding device with a 1:6 (wire: gap) ratio (see Fig. 3, process A1). The synthesis method for the PPy helix was derived from the previous work of the IMS group [24]–[26] and literature [21], [27]. For higher conductivity of the PPy film, it is paramount to clean the substrate electrode (Pt and Au-W) where the polymer deposition will happen. Hence, the Pt wire with the Au-W spacer was cleaned electrochemically in 2 M H_2SO_4 by polarizing it against stainless steel mesh with - 1.5 V and + 1.5 V, 10 min for each (process A2). Before the electrochemical deposition (process A3), the substrate electrode was conditioned in the synthesis solution for 40 min.

Synthesis: Galvanostatic electropolymerization (BioLogic BP-300) in a two-electrode cell was conducted at temperature -15°C (Lauda Proline RP 1845 cryostat) with a current density of 0.1 mA cm^{-2} for 17h (the first 10 min with 10% of current density, i.e., 0.01 mA cm^{-2}). The synthesis solution consisted of 0.2 M NBu_4PF_6, 0.2 M Py, and 2 w/w% MilliQ in PC. After synthesis, PPy (deposited on the Pt and Au-W template) was washed with ethanol and deionized water, then air-dried for 20 min. Next, the structure was transferred into the actuation solution of 0.2 M LiTFSI in PC. Using different electrolytes in synthesis and actuation is a common practice (e.g., in [28]). Finally, the Au-W wire spacer was carefully removed, creating filament-induced fracturing (process A4 and sections B and C). Since the PPy deposits on both the Pt and Au-W wires evenly, the filament-induced fracturing (C1) creates a ridged cross-section (highlighted on the SEM image B2, close-up on B3, and schematically drawn on C2). Afterward, the helix was reinserted into the actuation solution.

B. Characterization

Dynamic behavior: Two experiments were performed in parallel – the PPy-helix was cycled with driving voltage with a potentiostat to record both the current behavior (Cyclic Voltammetry – CV) and actuation behavior (motion detection analysis) with a camera (see Fig. 4, Section A).

Charge-transfer kinetics: The electrochemical properties were studied using the CV technique, a widely used method to study electrode (in this case, the PPy-helix) kinetics [29]. The voltage was swept between +0 V to +1 V (vs. Ag-AgCl/KCl 3 M) at least five times at a scan rate of ± 3 mV s^{-1}, maintained using an Ag-AgCl 3 M KCl reference electrode (RE). The electric circuit was completed using a 1 mm diameter carbon pencil core as the counter electrode (CE) (see Fig. 4 Section A for the electrode configuration).

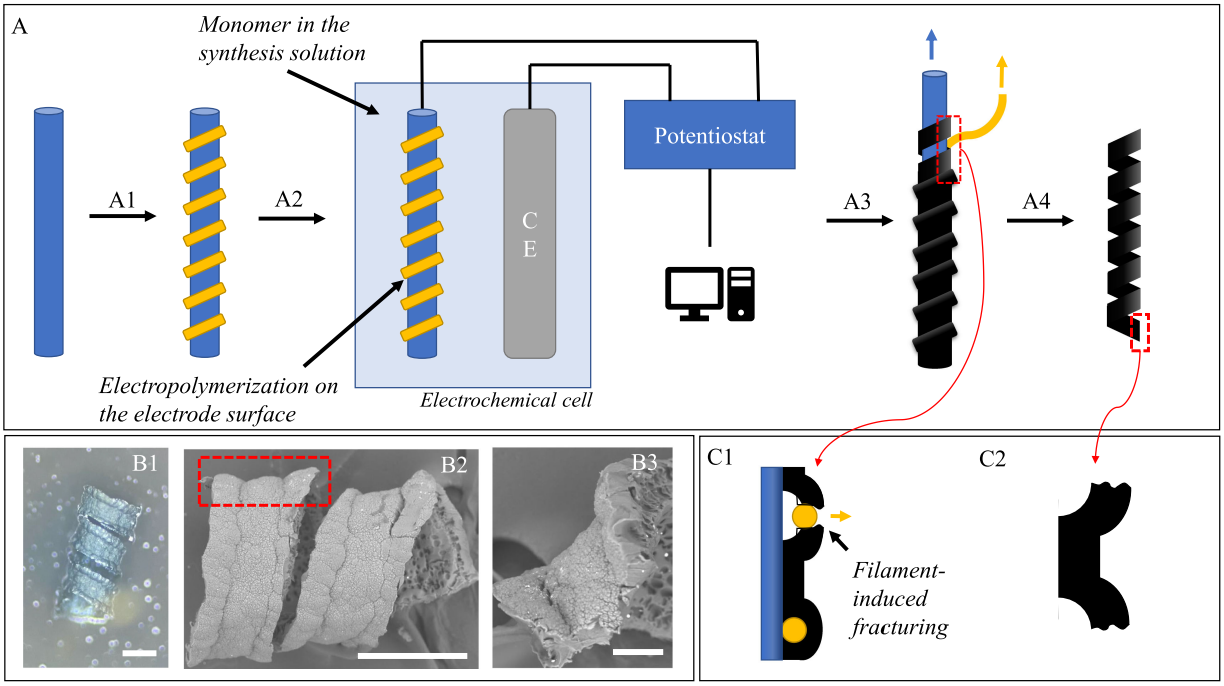

Fig. 3. The fabrication method of the PPy helix. Section A – preparation of the substrate electrodes and synthesis of the polymer, finishing with the removal of the substrate. Pt – blue, Au-W wire – yellow, PPy – black. Section B – the optical and scanning electron microscopy images of the PPy helix. Scale bars B1 and B2 – 250 μm; B3 – 50 μm. Section C – the formation of the ridged cross-section of the PPy ribbon that forms the PPy helix.

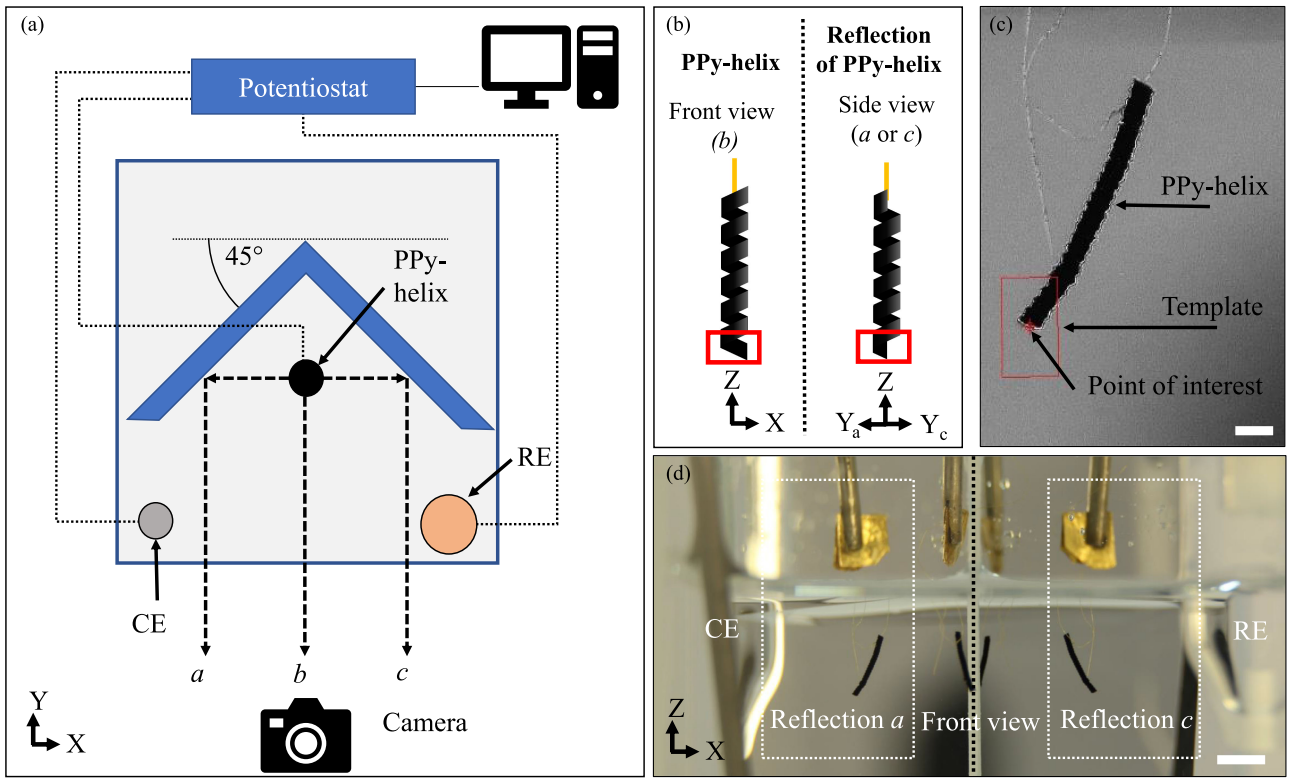

Fig. 4. The experimental setup. Section A – Top view of the measurement setup. The PPy-helix, CE, and RE are connected to the potentiostat for CV. The mirror (in blue) is positioned so that the optical paths (a, b, and c) can be used for 3D motion detection. Section B – the three dimensions for the motion detection analysis are derived from the two 2D images of the helix. Section C – the snapshot from the motion detection analysis Scale bar – 1 mm. Section D – the optical image of the actuation cell. Scale bar – 5 mm.

Motion: In parallel with the electrochemical characterization, the motion of the actuator was detected via camera and post-processed with an in-house LabVIEW program. A custom-made setup of the actuation cell incorporated two mirrors under 90° to each other and placed at 45° to the camera, allowing simultaneous view on all three dimensions of the actuator (see Fig. 4, Section A and D). A camera was set up in a way that both reflections and the actual actuator were in focus, and time-lapse (1 image per 10 s) of the actuation was recorded. The motion characteristics were extracted using the Grayscale Value Pyramid pattern-matching algorithm included in the Vision Development module in LabVIEW. A characteristic feature on the helix (i.e., the tip) was selected as the template. The template's center point coordinate was tracked across the time-lapse, resulting in a frame-by-frame pixel coordinate. A 3D displacement corresponding to each image in the series was achieved by matching the displacement data from the actual actuator and its reflection (see Fig. 4, Section B and C). The resulting displacement data was used to determine the linear strain of the actuator. The tip rotation was determined by comparing maximum and minimum rotation snapshots.

Compliance: PPy-helix covered with the electrolyte solution was investigated with a stress-strain measurement setup consisting of a force sensor (TRI202PAD, Panlab), a linear stage (Thorlabs), and a camera (see Fig. 8 Section B). The stage was actuated at 0.01 mm s^{-1}, and the resulting restoring force was measured.

IV. Results

A. Morphology of the Helix

The optical and SEM images of the dried helix show the well-known 'cauliflower' structure of the PPy as well as a relatively porous inner surface (Fig. 4, Section B). The morphological differences between outer and inner surfaces (active and passive, correspondingly) are evidence of 10x different applied current densities (0.01 mA cm^{-2} vs. 0.1 mA cm^{-2}, see experimental Section). A small morphological difference was also observed on the inner surface, depending on the substrate (PPy deposition on Au-W or Pt).

B. Multi-mode Actuation of the PPy-Helix

The linear strain of the PPy-helix was measured as 3D linear displacement between the two end-points of the actuator (see Fig. 5). The original length L was increased by ΔL, resulting in an 8% strain ($\Delta L/L$). Due to self-commutation (marked with blue arrows on Fig. 5), the PPy-helix could be approximated at any time-snapshot as a tube (see Video 1). Some minor gaps in the helix (marked with red arrows) were due to filament-induced fracturing defects or induced by strain during elongation. The tip rotation was determined to be approximately 180° (corresponding to voltage scan from 0 to 1 V at 3 mV s^{-1}).

The multimode actuation of the PPy-helix has potential in various microscale gripping applications as the combination of strain and rotation enables the gripper to anchor to the object via 'corkscrew'-like movement. The actuation bandwidth enables conformation to the movements and stimulating growth of living guests, suggesting potential in bioscaffolding applications.

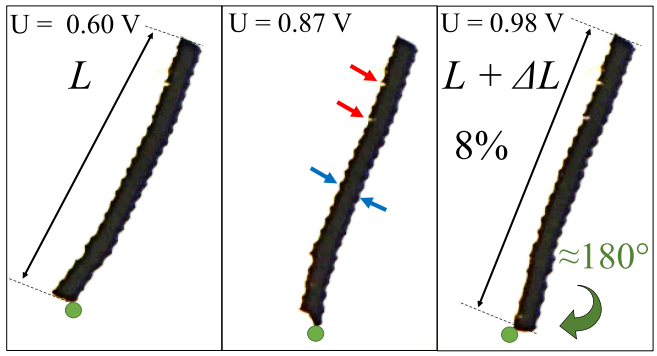

Fig. 5. Representative shapes of the PPy-helix in original length (L, left), halfway through motion (middle), and maximum length and rotation ($L + \Delta L$, 180° rotation, right). The arrows in the center image indicate minor infrequent gaps where the coils are not self-commutated. Both linear (8%) and rotary (180°) displacements are clearly observed.

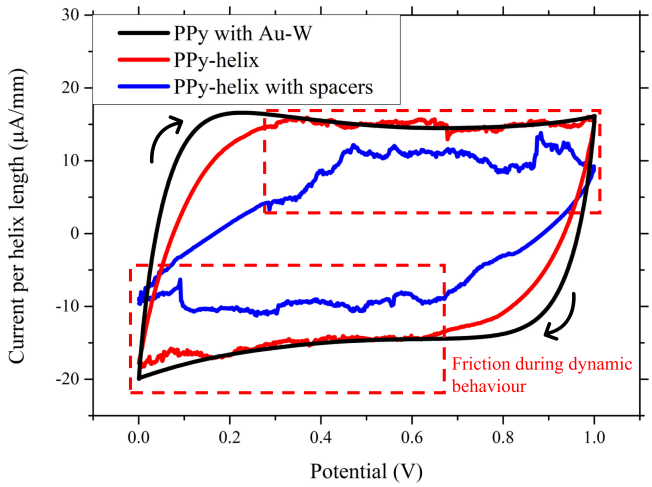

Fig. 6. The CV of the PPy-helix with and without markers (5th cycle). For comparison, the PPy helix with the Au-W spacer wire is also shown. The friction due to self-commutation can be seen in areas that correspond with dynamic behavior (marked with red). Arrows show the voltage cycling direction.

C. Self-Commutation: Cross-Turn Friction

The voltage scan of the PPy-helix generally showed a capacitor-like behavior with a rectangular cyclic voltammogram shape (see Fig. 6). The capacitor-like behavior is desired, as it indicates good access by the counter-ions and allows for simple voltage-driven charging control. No identifiable current peaks that would mark the presence of irreversible (redox) reactions were observed. Irreversible reactions during the deployment of the actuator are undesired as they could compromise material stability in cycling. Indeed, the CV and transient measurements (Fig. 6 and Fig. 7) showed no degradation in cycling. However, noise on the upper and lower current platoons can be seen on the current behavior of the helix compared to a uniform reference PPy (before fracture, i.e., a tubular actuator with the helical Au-W wire spacer still attached). The static can be interpreted

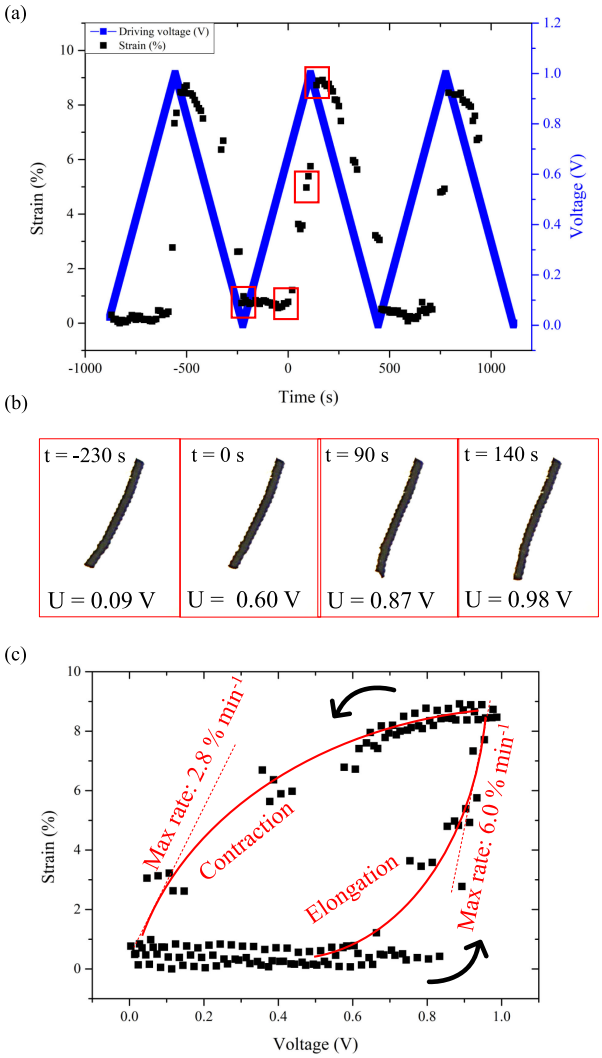

Fig. 7. The bi-stable behavior of the PPy-helix (cycles 3-5). Section A – resulting strain and driving voltage vs. time. Section B – image set of an elongation phase of the PPy-helix actuation cycle. Images correspond to the highlighted data in A. Section C – visualizing strain vs. driving voltage shows the different strain rates for elongation and contraction. The arrows show the voltage cycling direction. Note that the full actuation cycle (0 V to 1 V to 0 V) took ca 11 min (667 s).

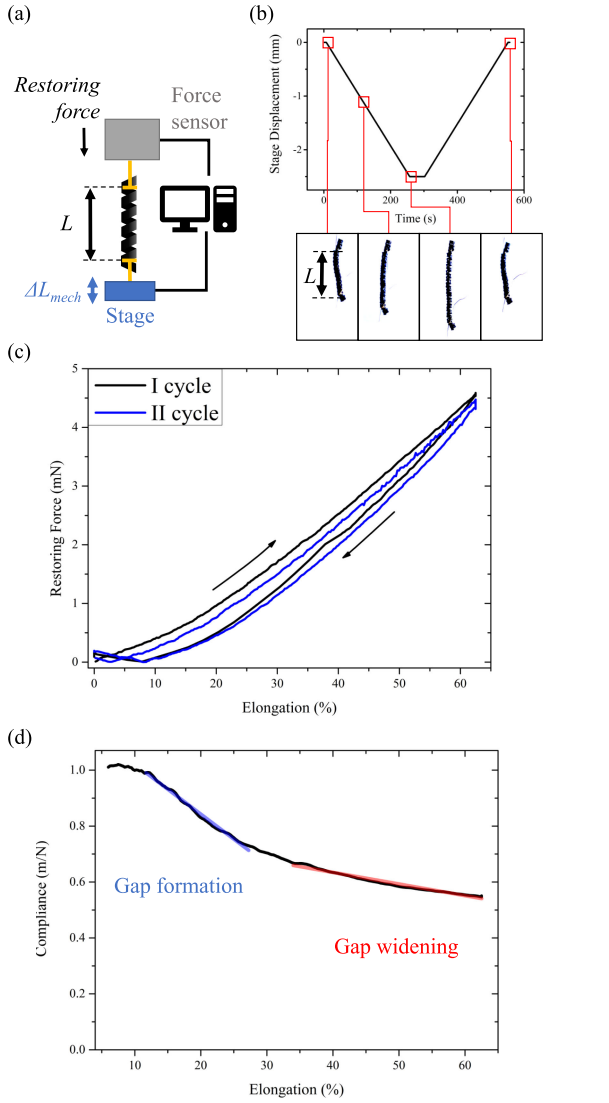

Fig. 8. Section A – the experimental setup. A linear stage applies strain on the PPy-helix with the other end attached to a force sensor (measuring the restoring force). Section B – stage movement profile and the corresponding snapshots of the helix elongation. Section C – cyclic stress-strain plot of the PPy helix, showing good repeatability. Section D – strain-dependent compliance of the PPy-helix. Two linear phases can be observed, corresponding to the initial gap formation between the helix's coils (in blue, y = -0.00415x+0.80051) and the increase of gap size between the coils (red, y = -0.01783x+1.19904). A moving average over 5 points was used to smooth the data.

as friction between the helix's spirals during dynamic movement (i.e., strain and rotation) as this random aperiodic signal component is missing in the reference (tubular) actuator. The tubular reference actuator had an overall maximum strain of 2% and did not exhibit tip rotation – this is expected, as the PPy filling the gaps between Au-W wires engaged only a part of the strain energy for displacing the Au-W helix (thus a lower total strain at the tip) and could not contribute to rotation due to the tubular shape (the bilayer structure could only contribute to a (negligible) increase in tube diameter, not translating into tip actuation). Two non-conductive plastic foil spacers were added to the PPy-helix to showcase the importance of self-commutation – we roughly estimate the magnitude of resistance increase to be 50%, as evidenced by increased amplitude of noise current (possibly due to PPy-to-PPy and PPy-to-plastic-foil friction). Although the performance was reduced, the spacers did not fully interrupt the functionality of the gripper, allowing for the potential gripping of objects between the coils of the helix. This concludes that the self-commutating super-structure is important but not critical in the work of the helical PPy ribbon, not unlike the folding in a protein.

D. Self-commutation: Bi-stable Actuation

The driving voltage and the resulting strain plotted versus time (see Fig. 7, Section A) confirms that the system is anion-active – positive strain is complementary to potential increase (the charge was compensated by anion influx). The resulting strain lags significantly behind the driving voltage. As seen from Fig. 7(image series B and strain vs. voltage in Section C),

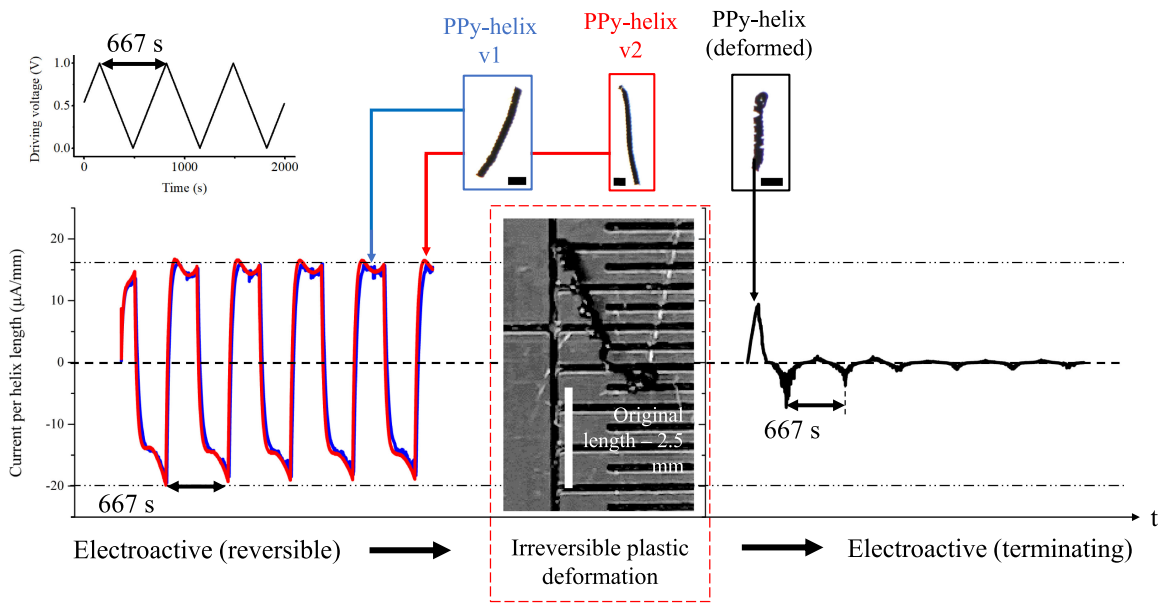

Fig. 9. The reversible and (highly) repeatable electroactive properties (both in time and cross-samples) of the PPy-helix are damaged when the helix is strained to a length increase of 100% (applied 200–300% strain, not measured). Scale bar – 1 mm.

the strain behavior exhibits bi-stable characteristics: negligible strain from 0 to 0.6 V was followed by rapid elongation (max rate 6.0% min^{-1}). The bi-stable behavior was about twice less pronounced in contraction (max rate 2.8% min^{-1}). This bi-stable behavior is estimated to be caused by friction between the self-commutated spirals of the helix – the ridged and ragged fractured edges of the coils self-lock until the volume change reaches a critical point and the edges are released in rapid succession. Positive volumetric change forces the edges of the coils into stronger mechanical contact with each other, whereas a negative volumetric change decreases the contact force, resulting in a different strain rate for elongation and contraction.

E. Compliance

Upon successful anchoring, the helix assumes a passive compliance function, enduring high structural strain. To demonstrate this phase, the PPy-helix was strained by an external force, and the resulting restoring force on the PPy-helix was measured (see Fig 8, Section A for experimental setup and B for the stage input signal and snapshots of the PPy-helix elongation, Video 1 for video). Note that there is no rotation of the helix as the helix is strained mechanically from the opposing ends. The PPy-helix showed elastomer-range structural strain with close to complete recovery (4% creep, acceptable for a fully polymeric material) from 63% mechanical strain (see Fig. 8, Section C). This highlights the material intelligence coded with the helical shape, as electroactive PPy is a relatively fragile non-thermoplastic material (strain-at-break usually under 10% [30]; up to 41.6% strain has been reported on a drastically plasticized highly conductive PPy, however, the electromechanical properties were not demonstrated [31]).

The compliance of the PPy-helix shows two distinct ranges: high compliance (0.7 m/N - 1.0 m/N) at moderate strains (<25%, dominated by initial gap formation between the helix's coils) and lower (0.55 m/N - 0.7 m/N) compliance at high strains (25–60%, dominated by the increase of gap size between the coils) (see Fig. 8 Section D, in blue and red, respectively). The strain-dependent compliance leaves design opportunities for leveraging dampening and energy storage.

F. In-shape Synthesis Assures Continuous PPy Network

The irreversibly electrochemically synthesized PPy-helix elongates and rotates upon activation and withstands elastic deformation. However, we observed a drastic loss in reversible electroactive behavior upon irreversible (plastic) deformation. Elongating the PPy-helix 200–300% (not measured) using external force (see Fig. 9) caused irreversible damage, and the actuator showed terminating electroactive properties: the helix showed rapid performance loss already at the very first cycle of electroactive actuation and degraded fully in only a few cycles. We hypothesize this was due to fracture of PPy chains in plastic deformation: upon application of electric input, the remaining intact PPy chains responsible for charge transfer experienced irreversible damage in the first post-deformation actuation cycles, likely due to an increased local current density. This served as proof that the super-structured self-commutating PPy-helix must be synthesized in-shape rather than in a thin film and later shaped into a helix. This fact severely limits the applicable common manufacturing techniques (extrusion, injection molding); to the contrary, template-assisted electrochemical synthesis is highly controllable with a close-to-100% yield, promising further scalability.

V. Conclusion

A multimode (linear-rotary) single-material (PPy) actuator for soft robotic application was designed, synthesized, and

characterized. The single-helix PPy ribbon was fully electrically controlled with a voltage range lower than 1 V and showed strain of up to 8%, tip rotation of ≈180°, and resilience to mechanical strain up to 63%. The learned principles for designing sub-mm-scale biomimetic structures using electropolymerized CP are as follows:

1) Filament-patterning and filament-induced controlled fracture approaches were effective for generating sub-mm 3D-structure in-shape, without plastic deformations that could damage the PPy electrical network. The same Au-W wire acted as a current-collector, pattern, and fracturing agent.
2) A ten-fold change in a single process parameter - current density – defines active and passive PPy volume, enabling the formation of interface-free functional gradients during synthesis without the need for delamination-prone assembly steps.
3) Self-commutation between the helix's coils (enhanced by swelling for increased contact tension) provides a favorable transmission of electronic charge as well as generated force along the spiral.
4) Friction during self-commutation is likely responsible for bi-stable actuation mode; the overall benefits of self-commutation outweighed the frictional losses.
5) The spiral shape yielded 4x higher linear actuation and an additional rotary axis of freedom, in contrast to the tubular structure with embedded filament.

Potential use cases can be found in bio-hybrid robotics as a biocompatible scaffold for bacteria, controlled entanglement, and snap-and-release applications.

REFERENCES

[1] K. Svennersten *et al.*, "Mechanical stimulation of epithelial cells using polypyrrole microactuators," *Lab Chip*, vol. 11, no. 19, pp. 3287–3293, 2011.

[2] C. E. Schmidt *et al.*, "Stimulation of neurite outgrowth using an electrically conducting polymer," *Proc. Nat. Acad. Sci. USA*, vol. 94, no. 17, pp. 8948–8953, , 1997.

[3] G. M. Spinks, "Advanced actuator materials powered by biomimetic helical fiber topologies," *Adv. Mater.*, vol. 32, no. 18, 2020, Art. no. 1904093.

[4] Y. Forterre and J. Dumais, "Generating helices in nature," *Science*, vol. 333, no. 6050, 2011, Art. no. 1715.

[5] C. S. Haines *et al.*, "Artificial muscles from fishing line and sewing thread," *Science*, vol. 343, no. 6173, pp. 868–872, 2014.

[6] S. Aziz *et al.*, "Fast and high-strain electrochemically driven yarn actuators in twisted and coiled configurations," *Adv. Funct. Mater.*, vol. 31, no. 10, 2021, Art. no. 2008959.

[7] T. T. Hoang *et al.*, "Bio-inspired conformable and helical soft fabric gripper with variable stiffness and touch sensing," *Adv. Mater. Technol.*, vol. 5, no. 12, 2020, Art. no. 2000724.

[8] S. Lee *et al.*, "A needle-type microrobot for targeted drug delivery by affixing to a microtissue," *Adv. Healthcare Mater.*, vol. 9, no. 7, 2020, Art. no. 1901697.

[9] M. Dong *et al.*, "3D-printed soft magnetoelectric microswimmers for delivery and differentiation of neuron-like cells," *Adv. Funct. Mater.*, vol. 30, no. 17, 2020, Art. no. 1910323.

[10] A. L. Pang, A. Arsad, and M. Ahmadipour, "Synthesis and factor affecting on the conductivity of polypyrrole: A short review," *Polymers Adv. Technol.*, vol. 32, no. 4, pp. 1428–1454, 2021.

[11] D. Melling, J. G. Martinez, and E. W. H. Jager, "Conjugated polymer actuators and devices: Progress and opportunities," *Adv. Mater.*, vol. 31, no. 22, 2019, Art. no. 1808210.

[12] J. M. McCracken, B. R. Donovan, and T. J. White, "Materials as machines," *Adv. Mater.*, vol. 32, no. 20, 2020, Art. no. 1906564.

[13] M. Golabi, A. P. F. Turner, and E. W. H. Jager, "Tuning the surface properties of polypyrrole films for modulating bacterial adhesion," *Macromol. Chem. Phys.*, vol. 217, no. 10, pp. 1128–1135, 2016.

[14] R.-B. Song *et al.*, "Living and conducting: Coating individual bacterial cells with in situ formed polypyrrole," *Angewandte Chemie Int. Ed.*, vol. 56, no. 35, pp. 10516–10520, 2017.

[15] D. Q. Le *et al.*, "Development of an observation platform for bacterial activity using polypyrrole films doped with bacteria," *Anal. Chem.*, vol. 87, no. 7, pp. 4047–4052, 2015.

[16] M. Golabi, A. P. F. Turner, and E. W. H. Jager, "Tunable conjugated polymers for bacterial differentiation," *Sensors Actuators B: Chem.*, vol. 222, pp. 839–848, 2016.

[17] X.-Y. Hu *et al.*, "Synthesis and characterization of the conducting polymer micro-helix based on the spirulina template," *Polymers*, vol. 10, no. 8, 2018, Art. no. 882.

[18] M. A. Zeeshan *et al.*, "Hybrid helical magnetic microrobots obtained by 3D template-assisted electrodeposition," *Small*, vol. 10, no. 7, pp. 1284–1288, 2014.

[19] R. Mutlu, G. Alici, and W. Li, "Three-dimensional kinematic modeling of helix-forming lamina-emergent soft smart actuators based on electroactive polymers," *IEEE Trans. Syst., Man, Cybern.: Syst.*, vol. 47, no. 9, pp. 2562–2573, Sep. 2017.

[20] T. Otero and M. Broschart, "Polypyrrole artificial muscles: A new rhombic element. Construction and electrochemomechanical characterization," *J. Appl. Electrochemistry*, vol. 36, pp. 205–214, 2006.

[21] S. Hara *et al.*, "Polypyrrole–metal coil composite actuators as artificial muscle fibres," *Synthetic Met.*, vol. 146, no. 1, pp. 47–55, 2004.

[22] G. Alici *et al.*, *Conducting Polymers as EAPs: Device Configurations*, Berlin, Germany: Springer, 2016.

[23] B. Yan *et al.*, "Intrinsically passivated polypyrrole/polyol-borate soft electroactuators," *Sensors Actuators A: Phys.*, vol. 293, pp. 200–206, 2019.

[24] R. Temmer *et al.*, "Combined chemical and electrochemical synthesis methods for metal-free polypyrrole actuators," *Sensors Actuators B: Chem.*, vol. 166-167, pp. 411–418, 2012.

[25] T. T. Khanh *et al.*, "Role of polymerization temperature on the performance of polypyrrole/dodecylbenzenesulphonate linear actuators," *Synthetic Met.*, vol. 247, pp. 53–58, 2019.

[26] R. Khadka *et al.*, "Role of polyethylene oxide content in polypyrrole linear actuators," *Mater. Today Commun.*, vol. 23, 2020, Art. no. 100908.

[27] W. Zheng, P. G. Whitten, and G. M. Spinks, "Polypyrrole actuators: The effects of polymer thickness and voltage scan rate on fractional charging and isotonic actuation strain," *Multifunctional Mater.*, vol. 1, no. 1, 2018, Art. no. 014002.

[28] M. Beregoi *et al.*, "Versatile actuators based polypyrrole-coated metalized eggshell membranes," *ACS Sustain. Chem. Eng.*, vol. 6, no. 8, pp. 10173–10181, 2018.

[29] R. G. Compton and C. E. Banks, *Understanding Voltammetry*, Singapore: World Scientific, 2018.

[30] F. Gao *et al.*, "Bioinspired design of strong, tough, and highly conductive polyol-polypyrrole composites for flexible electronics," *ACS Appl. Mater. Interfaces*, vol. 9, no. 7, pp. 5692–5698, 2017.

[31] F. Gao *et al.*, "All-polymer free-standing electrodes for flexible electrochemical sensors," *Sensors Actuators B: Chem.*, vol. 334, 2021, Art. no. 129675.